Steel and Composite Structures, *Vol. 31, No. 1 (2019) 27-41*
DOI: https://doi.org/10.12989/scs.2019.31.1.027

Shear lag effect in steel-concrete composite beam in hogging moment

Da Luo [1a], Zhongwen Zhang [*2] and Bing Li [3b]

[1] *College of Civil Engineering and Architecture, Guangxi University, Nanning 530004, P.R. China*
[2] *Key Laboratory of Concrete and Prestressed Concrete Structures of Ministry of Education, School of Civil Engineering, Southeast University, Nanjing 210000, P.R. China*
[3] *School of Civil and Environmental Engineering, Nanyang Technological University, Singapore 639798*

(*Received December 21, 2018, Revised March 9, 2019, Accepted March 17, 2019*)

Abstract. Shear lag effect can be an important phenomenon to consider in design of the steel-concrete composite beams. Researchers have found that the effect can be strongly related with the moment distribution, the stiffness and the ductility of the composite beams. For continuous composite beams expected to sustain hogging moment, the shear lag effect can be more distinct as cracking of the concrete slab reduces its shear stiffness. Despite its influences on behaviour of the steel-concrete composite beams, a method for calculating the shear lag effect in steel-concrete composite beams sustaining hogging moment is still not available. Shear lag effect in steel-concrete composite beams sustaining hogging moment is investigated in this paper. A method was proposed specifically for predicting the effect in the cracked part of the steel-concrete composite beam. The method is validated against available experimental data. At last, FE studies are conducted for steel-concrete composite beams with different design parameters, loading conditions and boundary conditions to further investigate the shear lag effect and compare with the proposed method.

Keywords: steel-concrete composite beams; composite structure; shear lag effect; truss analogy

1. Introduction

The shear lag effect is a phenomenon related with accumulation of the shear deformation in the section of bending structural members while transferring the longitudinal stress. Contrary to the plane section assumption which is commonly adopted in analyzing bending structural members, longitudinal strain in flange of the non-rectangular beam section can vary significantly due to this effect. The shear lag effect has received significant attention in recent research concerning steel-concrete composite beams. With a large, reinforced concrete slab connected with profile steel by shear connectors, this form of structure has good stiffness and moment capacity, and is often used as decks of bridges. Transverse dimension of the slab perpendicular to the profile steel beam can be quite large. When the flange of the composite beam is in tension or compression due to the bending moment, distribution of the longitudinal strain in the flange concrete is uneven, (Amadio *et al*. 2004, Henriques *et al*. 2015, Ding *et al*. 2016, Yang *et al*. 2016, Lasheen *et al*. 2018) and the distribution is distinctly influenced by the shear lag effect. (Dezi *et al*. 2003, Amadio *et al*. 2004, Pecce *et al*. 2012, Lee and Chiew 2013, Zhong *et al*. 2017, Boules *et al*. 2018) Correspondingly, stiffness, moment capacity, natural frequency and the distribution of bending moments in steel-concrete composite beams can be strongly affected. (Siekierski 2015)

For considering the effect in design, engineers generally use the concept of the effective width which assumes only a portion of the concrete flange is mobilized in resisting the sectional moment. In Eurocode 4 (ENV 1994-1-1 1994), the effective width of the slab is related to span of the beam between the points of zero bending moment, distance of the shear connector and the geometric flange width. The effective width at the end of the beam is also different from the other location. The existing method was often found to be quite conservative and over-simplified by researchers. (Amadio *et al*. 2004, Aref *et al*. 2007, Castro *et al*. 2007, Goncalves and Camotim 2010, El-Shihy *et al*. 2010, Lee and Chiew 2013, Gara *et al*. 2014, Xiang and He 2017, Lasheen *et al*. 2018) Also, researchers found that influences of the shear lag effect can be more complicated in continuous steel-concrete composite beams. (Amadio *et al*. 2004, Sun *et al*. 2014) For these beams, hogging moments are expected around supports in the mid-span and significant cracks can exist in these areas. Aref *et al*. (2007) pointed out that the current practice of using similar definition of effective width for hogging and sagging moment zones is problematic and proposed different definitions of the effective flange width accordingly. Researchers also found that the shear lag effect is more severe in the cracked part of the composite beam while sustaining the hogging moment. (Chiewanichakorn *et al*. 2004) Researchers observed that cracks distinctly reduce shear stiffness of the concrete panels. (Beyer *et al*. 2011, Kim and Mander 1999, 2007, Ju *et al*. 2013) As the shear

*Corresponding author, Associate Professor,
E-mail: zwzhang@seu.edu.cn
[a] Ph.D. Student, E-mail: luoda@gxu.edu.cn
[b] Associate Professor, E-mail: cbli@ntu.edu.sg

ISSN: 1229-9367 (Print), 1598-6233 (Online)

lag effect is related with shear stiffness of the section (Kwan 1996, Gao *et al*. 2016), the more severe shear lag effect in the cracked part of the beam is expected.

Shear stiffness of the cracked concrete panels can often be predicted by the truss analogy. The truss analogy has been proposed in 1902 and was continuously used and improved by researchers. (Kim and Mander 1999) Important recent developments of the truss analogy include the modified compression field theory proposed by Vecchio and Collins (1986) capable of considering strength and softening of the concrete in compression and tension and the strut-and-tie model used by MacGregor *et al*. (1997) for predicting shear strengths of the deep beams. Paulay (1971), Kim and Mander (1999), used the truss analogy to calculate the shear stiffness and deformation in cracked concrete members. The method has also been used to predict shear strength and stiffness of concrete members sustaining large inelastic deformation including the work done by Hines and Seible (2004), Beyer *et al*. (2011) and Moharrami *et al*. (2015).

Using the truss analogy, this paper proposes a method for calculating the shear lag effect in sections of the steel-concrete composite beams sustaining hogging moment. The proposed method was compared with experimental results. For further investigation of the shear lag effect in steel-concrete composite beams and validation of the proposed method, finite element (FE) models were built for steel-concrete beams with various parameters. The shear lag effect in multi-span continuous steel-concrete composite beams with different loading combinations was also investigated by the FE models comparing with proposed method.

2. Proposed method

2.1 Truss analogy for cracked concrete slab in steel-concrete composite beam

Used properly, models based on truss analogy can estimate shear strength and stiffness of the cracked concrete panels effectively. The truss models have been under consistent development and researchers can use very different assumption in modelling the concrete members by the truss. (Kim and Mander 1999) However, the central idea of the analogy is rather straightforward which is to represent the concrete struts sustaining diagonal compression stress field as the diagonal chord while the reinforcing bars in tension connecting the concrete struts are represented by the horizontal tension chords. These diagonal and horizontal chords are connected by vertical chords in tension or compression modelling the longitudinal reinforcing bars or the vertical compression stress flow in the concrete. Depending on state of the compression stress in the cracked member, the diagonal chords can be assumed to be parallel to each other with a constant angle with the horizontal chords. Otherwise, the angle between the horizontal and diagonal members can vary to model the stress state of the concrete member more realistically. (Hines and Seible 2004) The forces of the chords of the truss should be in equilibrium with each other and the external load sustained by the concrete member. The geometric compatibility between deformation of the chords sustaining load can be ignored or considered. The compatibility is often ignored in models calculating shear strengths of concrete members using the truss analogy such as the strut-and-tie models. In calculating shear stiffness of the cracked members, on the other hand, both the compatibility and the equilibrium should be considered. Using energy method to solve the compatibility and equilibrium equations, deformation of the truss system can be calculated which approaches deformation of the cracked concrete member it represents. Kim and Mander (1999) used different kinds of truss analogies for predicting shear stiffness of flexural concrete members. The accuracy was found to be satisfactory even when very simple kind of truss was used for the flexural concrete member.

Similar truss analogy was used for calculating the shear stiffness and the shear lag effect in the cracked concrete slab in the steel-concrete composite beam in this paper. A relatively simple case was considered for deducing the equation in which the edge of the slab is connected with the profile steel while the longitudinal reinforcing bars are concentrated at the two ends of the slab as shown in Fig. 1. A truss analogy was used to calculate the cracked slab as shown in Fig. 2. The assumptions made in calculating the truss include ignoring tensile strengths of the concrete, a constant angle of θ between the horizontal chords and the diagonal chords and a constant distance between the horizontal truss members similar with that of the shear connectors. Therefore, the longitudinal reinforcement, the transverse reinforcement and the diagonal concrete struts are represented by the vertical trusses, the horizontal trusses and the diagonal trusses, respectively as shown in Figs. 1-2. The assumptions made are similar to some other researchers in calculating shear stiffness of flexural concrete members. (Kim and Mander 1999, Pan and Li 2013, Pan *et al*. 2014) However, the load applied to the truss is different. For the concrete slab, the shear forces are transferred to truss joints though shear connectors. Validity of these assumptions and the truss analogy will be discussed afterward with comparisons with experimental results and the FE analyses.

Considering a simplified case in which the truss is resisting an individual force of dF transferred from a shear connector shown in Fig. 2, only a part of the truss will be mobilized in resisting dF. The truss system can be simplified

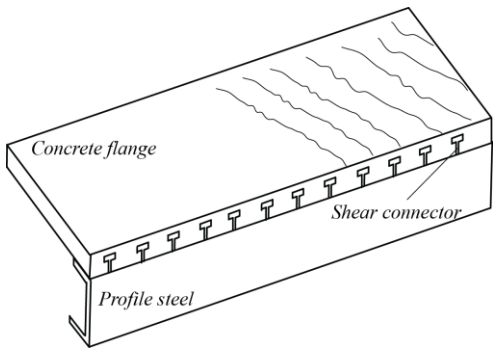

Fig. 1 Cracked concrete flange sustaining hogging moment

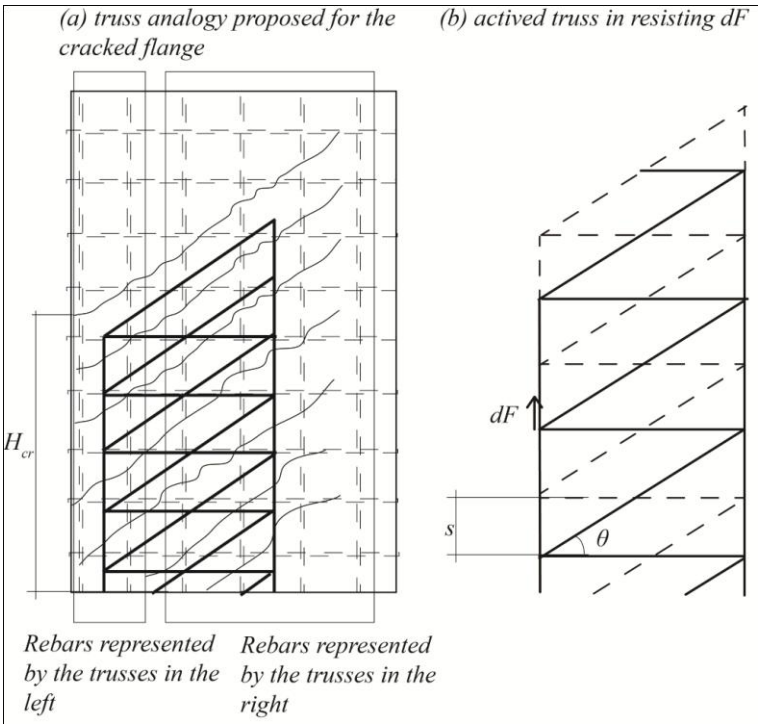

Fig. 2 Proposed truss analogy for the cracked concrete and the mobilized force by an individual d*F*

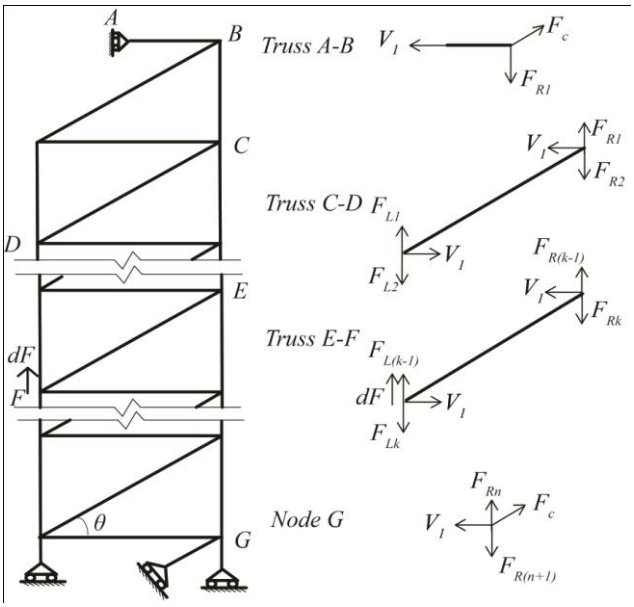

Fig. 3 Force equilibrium of the proposed truss

to Fig. 3. (Kim and Mander 1999) Based on equilibrium of the forces, the internal forces in every truss member can be expressed in terms of *dF* and V_1, the shear force in the horizontal members as shown in Fig. 3. The strain energy of the truss system can be expressed as

$$U = \sum_{k=1}^{n+1} \frac{V_1^2 \cdot jd}{2E_s A_s} + \sum_{k=1}^{n} \frac{V_1^2 \cdot jd}{2\cos^4\theta \cdot s \cdot t \cdot E_c} + \sum_{k=1}^{n} \frac{k^2 V_1^2 \cdot jd \cdot \tan^3\theta}{2E_s A_R} + \sum_{k=1}^{n_1-1} \frac{k^2 \cdot V_1^2 \cdot jd \cdot \tan^3\theta}{2E_s A_L} + \sum_{k=n_1}^{n-1} \frac{(dF - k \cdot V_1 \cdot \tan\theta)^2 \cdot jd \cdot \tan\theta}{2E_s A_L} \quad (1)$$

With $n = \frac{H_{cr}}{jd \tan\theta} + 1$

in which *jd* is the length of horizontal ties; E_s is the Young's modulus of the reinforcing bars; E_c is the modulus of the concrete; *t* is the thickness of the flange; *s* is the vertical distance of the truss assumed as the vertical distance of the horizontal reinforcing bars in the flange; A_s is the area of the horizontal reinforcing bars in the distance of the assumed horizontal truss; A_L and A_R are the areas of the concentrated reinforcing bars in the two ends of the flange, respectively; n_1 is the node number where the d*F* is, which start at the top-left of the truss (n_1 is 1 for the top-left node of the truss and is *n* for the bottom-left node of the truss.). Based on Castigliano's second theorem, Eq. (2) can be deduced which relates the variation of the tension forces in the vertical members with the applied d*F* to the truss

$$\frac{V_1}{dF} = \frac{\left[3n(n-1) - 3n_1(n_1-1)\right]\tan^2\theta}{\frac{6(n+1)A_L}{A_s} + \frac{6nA_L E_s}{\cos^4\theta \cdot stE_c} + \frac{n(n+1)(2n+1)A_L}{A_R} + (n-1)n(2n-1)\tan^3\theta} \quad (2)$$

For the dF considered, variation of the tension forces in the vertical trusses in the right is given in Fig. 4(a). With Eq. (2) these forces can be calculated.

2.2 The shear lag effect in steel-concrete composite beam

For a loaded beam shown in Fig. 1, diagonal cracks in the concrete flange exist in locations where the bending moment of the beam exceeds the cracking moment M_{cr} determined by tensile strength of the concrete and moment of inertia of the section. The longitudinal reinforcing bars are resisting some tension forces at cracking of the flange, and the proposed truss is resisting some vertical force at the top introduced by these tension forces. (F_{Rcr} shown in Fig. 4) As the hogging moment increases along span of the beam, the section of concrete flange resists more and more tension forces which are transferred to the flange by the shear connectors. Increases of the tension forces in the vertical truss members, therefore, are determined by the forces of the connectors and stiffness of the truss as calculated by Eq. (2). Before significant yielding of the reinforcing steel and the cracked concrete, a linear superposition can be used. If distribution of the forces in the connectors is known, forces in the vertical trusses in the right can be calculated as shown in Fig. 4 with the increment of internal force of the right vertical truss

$$\Delta F_R = \tan\theta \sum_{K=1}^{N} V_1(K) \tag{3}$$

Multiple methods are available for calculating forces in the shear connectors for steel-concrete composite beams including the proposed method by Qi *et al*. (2017). Generally, these forces depend on stiffness of the shear connector and the slip between the concrete flange and the profile steel. (Chiorean and Buru 2017, Bezerra *et al*. 2018) For continuous steel-concrete composite beams, the concrete flange can resist tension or compression forces depending on bending moment resisted by the beam (Fang *et al*. 2016). Forces in the shear connectors also change accordingly. For a simple beam, the shear force in the connectors on the symmetrical plane must be zero, and the shear forces of the other connectors gradually increase with slip between the concrete flange and the profile steel. Therefore, a simple linear distribution of dF is assumed for the truss with the force adjacent to the support being minimal (Fig. 4). Therefore, the proposed truss corresponds to the cracked concrete flange from the location of symmetrical plane to the starting of cracks in the concrete flange. An explicit expression can also be derived

$$\begin{aligned}\Delta F_R &= \tan\theta \sum_{K=1}^{N} V_1(K) \\ &= \alpha \tan\theta F_m \left[\begin{array}{l} (2n-1)s^2 \dfrac{N(N+1)(2N+1)}{6\,jd\tan\theta \cdot H} \\ -s^3 \dfrac{N^2(N+1)^2}{4(jd\tan\theta)^2 H} \end{array} \right]\end{aligned} \tag{4}$$

With $\alpha = \dfrac{3\tan^2\theta}{\dfrac{6(n+1)A_L}{A_s} + \dfrac{6nA_L E_s}{\cos^4\theta \cdot stE_c} + \dfrac{n(n+1)(2n+1)A_L}{A_R} + (n-1)n(2n-1)\tan^3\theta}$;

$N = \dfrac{H_{cr}}{s}$.

Where F_m is the maximum shear force of all connectors.

With ΔF_R known, the tension force of the right vertical truss in any location of the cracked flange can be approximately calculated as (Fig. 4)

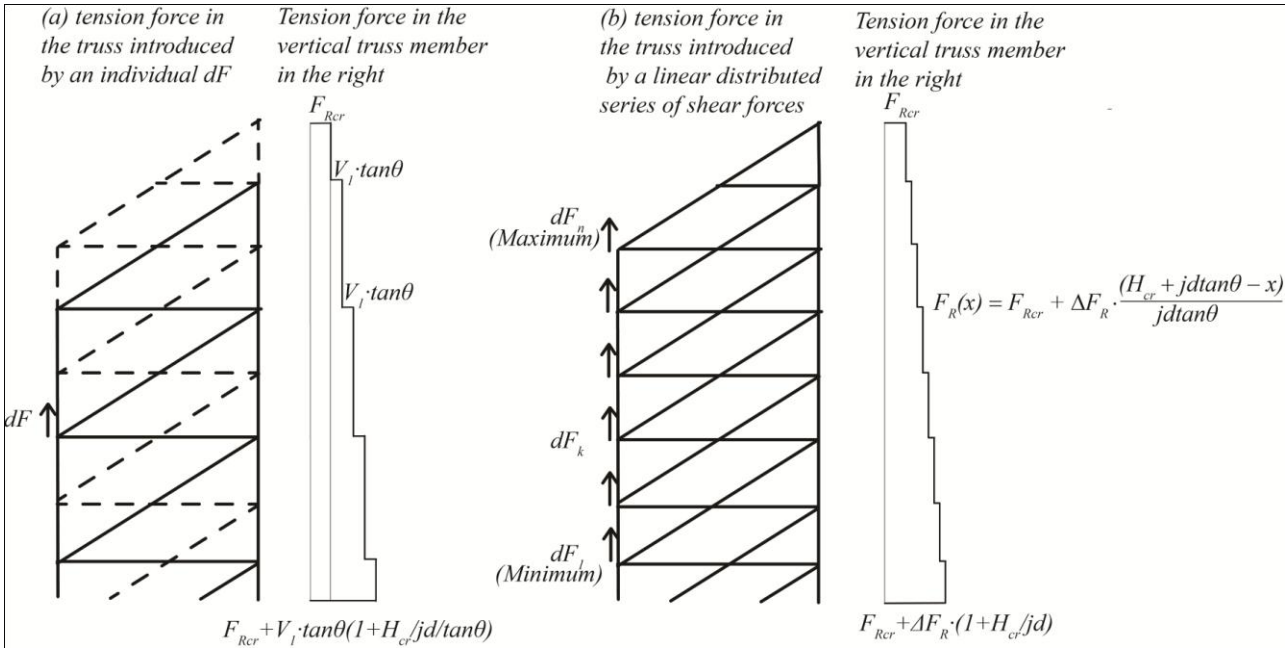

Fig. 4 Tension force in the right trusses due to an individual and a linearly distributed series of dF along the shear connectors

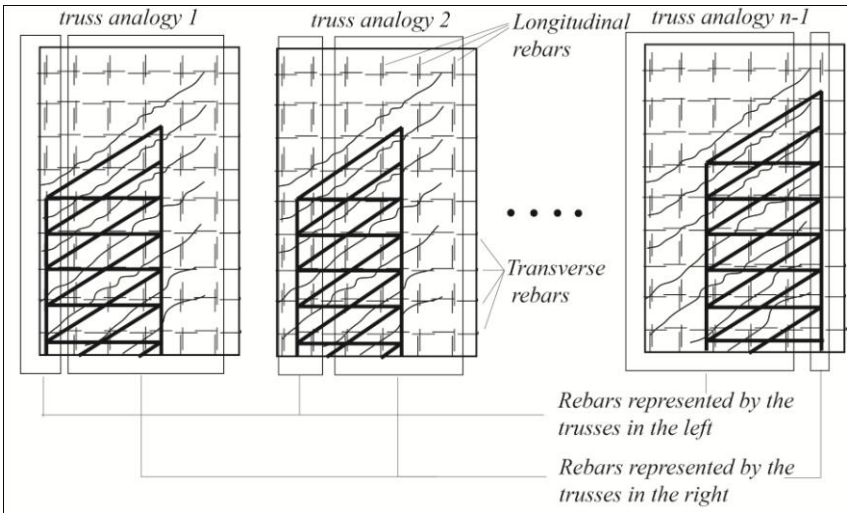

Fig. 5 Truss analogy corresponding to different assumption of distributed reinforcing bars

$$F_R(x) = F_{Rcr} + \Delta F_R \cdot \frac{(H_{cr} + jd\tan\theta - x)}{jd\tan\theta} \tag{5}$$

F_{Rcr}, the tension force of the right vertical truss at cracking can be regarded as the right portion of shear force which are transmitted by the shear connectors in the non-cracking area.

$$F_{Rcr} = \frac{A_R}{A_L + A_R} \cdot \int_{H_{cr}}^{H} ddF = \frac{A_R}{A_L + A_R} \cdot \frac{H^2 - H_{cr}^2}{2sH} F_m \tag{6}$$

In the equation, H can be regarded as half of the span of the beam. So the forces of the left vertical truss at any location of the cracked flange is

$$\begin{aligned} F_L(x) &= F_{fl}(x) - F_R(x + jd\tan\theta) = F_{fl}(x) - F_R(x) + \Delta F_R \\ &= F_{fl}(x) - F_{Rcr} - \Delta F_R \frac{H_{cr}}{jd\tan\theta} + \Delta F_R \frac{x}{jd\tan\theta} \end{aligned} \tag{7}$$

With $F_{fl}(x) = \int_x^H ddF = \frac{H^2 - x^2}{2sH} F_m$

Eq. (7) was proposed assuming the longitudinal reinforcing bars were represented by the two chains of vertical trusses shown in Fig. 2. As a matter of fact, the equation can be used assuming any combination of longitudinal reinforcing bars represented by the left vertical trusses or the right vertical trusses. Therefore, n-1 ratios can be derived for n vertical reinforcing bars (Fig. 5). Assuming the stress in the ith longitudinal reinforcing bars to be s_i and area of the ith reinforcing bar to be A_i, these equations can be written for

$$R_k = \frac{\frac{F_{Rk}}{A_{Rk}}}{\frac{F_{Lk}}{A_{Lk}}} = \frac{\sum_{j=k+1}^{n} s_j A_j \cdot \sum_{i=1}^{k} A_i}{\sum_{i=1}^{k} s_i A_i \cdot \sum_{j=k+1}^{n} A_j} \tag{8}$$

with $k \in (1, n-1)$

Solving the set of equations, stress in each of the reinforcing bars can be calculated and expressed in terms of s_1, the stress in the reinforcing bar adjacent to the shear connectors. Therefore, the differences of the stresses in the longitudinal reinforcing bars caused by the shear lag effect can be calculated. The effective width can therefore be calculated from Eq. (6) based on the method proposed by Aref *et al*. (2007) or the method adopted by Amadio *et al*. (2004). For Beam 1 tested by Amadio *et al*. (2004), Eq. 6 predicts the η ratio (η is calculated as the portion of the effective width compared with the geometric flange width as defined by Eq. (6) in Amadio *et al*. (2004).) to be 0.64 compared with the experimental determined minimal value of 0.57. Alternatively, the R_{sle} ratio can be used to characterize the shear lag effect in the concrete flange as

$$R_{sle} = \frac{\sum \varepsilon_i A_i}{\varepsilon_w \sum A_i} \tag{9}$$

with ε_i and A_i being the strain and area of the ith longitudinal reinforcing bars in the flange respectively and ε_w being the strain in the part of the flange adjacent to the shear connector. The R_{sle} ratio can be useful if elements adopting the plane section assumption is used for analysing the steel-concrete composite beams such as the fibre beam column element or the nonlinear beam column model. The ratio can be used to reduce the longitudinal strain calculated for the reinforcing bars in the flange based on the plane section assumption.

2.3 Comparison of the proposed method with experimental results

Using the proposed model, shear lag effect of some tested specimens was calculated and compared with the experimental results. Limited to the experimental data reported strains in the longitudinal reinforcing bars, five specimens were found from two different sources. They are the Specimen SB9, SB10 and SB11 reported in Nie *et al*. (2007) and 4GHFCOM and 4GHFCON reported by

Table 1 Comparisons of the experimental and calculated R_{sle} ratio

	Load level	0.5yield	0.75yield	1.0yield
SB9	Calculated	0.97	0.93	0.88
	Experimental	0.99	0.92	0.85
	Load level	0.5yield	0.75yield	1.0yield
SB10	Calculated	0.94	0.88	0.82
	Experimental	0.93	0.89	0.76
	Load level	0.5yield	0.75yield	1.0yield
SB11	Calculated	0.91	0.85	0.78
	Experimental	0.95	0.94	0.82
	Load level	0.5yield	0.95yield	
4GHFCOM	Calculated*	0.83/0.72	0.76/0.65	
	Experimental*	0.90/0.63	0.77/0.46	
	Load level	0.5yield	0.95yield	
4GHFCON	Calculated*	0.83/0.72	0.76/0.65	
	Experimental*	1.12/0.81	1.12/1.00	

Carpenter *et al*. (2005). Shear lag effect were calculated from strains in the longitudinal bars in these specimens at different load levels based on Eq. (9). Taking the Specimen SB10 as an example, H of the specimen is equal to 1.9 m for SW10. H_{cr} corresponds to the location where the tensile stress in the top surface of concrete flange reaches the cracking strength. For the specimen, only the thinner concrete height is considered in the calculation. The distance of SB10 from the neutral axis to the concrete surface is 90 mm. and the cracking moment is calculated as 14.7 kN·m. According to the moment distribution diagram, the crack height H_{cr} corresponding to different load levels can be determined for the specimen. The observed cracking angle in the test is between 15 and 45 degrees, so 30 degree of cracked angle is used. The number of reinforcing bars at one side of the slab is 4. Therefore, 3 combinations of reinforcing bars were considered in using Eq. (7) which gives 3 ratios as shown in Eq. (8). The portion of the strains in the reinforcing bars can therefore be calculated based on Eq. (9). Results of the comparison are shown in Table 1. As the table shows, the proposed method captures the shear lag effect in the Specimen SB9, SB10 and SB11 well. The maximum error was within 10% of the experimental results. The reducing tendency of the R_{sle} ratio with increase of the load was also predicted. Two pieces of profile steel are used for the Specimen 4GHFCOM and 4GHFCON. The shear lag effect is calculated for the overhanging part of the slab and the middle part of the slab independently. Moreover, strains were not reported for all longitudinal reinforcing bars in 4GHFCOM and 4GHFCON. The missing strains were assumed using a linear interpolation from the reported strains in the adjacent bars. This could be partially responsible for the differences between the calculated and experimental R_{sle} ratios for 4GHFCOM in Table 1. For 4GHFCON, a larger error was found for the proposed equation. This is probably related with the distribution of shear connectors in 4GHFCON. For the specimen, the shear connectors only exist in a limited part of the span of the beam, which violates assumption of the distributed shear connectors in deducing the equation. The shear lag effect is therefore less severe than anticipated.

3. Finite element model for shear lag effect in steel-concrete composite beams

3.1 Verification of finite element method

The experimental data available regarding shear lag effect in composite steel-concrete beams are rather limited compared with the various design parameters affecting the shear lag effect. For further investigations of the effect, FE analyses were performed with consideration of the material nonlinearity, cracking and slipping between the flange and the profile steel. The FE models were built in TNO Diana 9.6. (TNO Diana 2014) The concrete flange was modelled by 8 nodes isoparametric brick elements (HX24L) with embedded reinforcing bars. The profile steel, with its equivalents thickness, was modelled by 4 nodes curved shell elements (Q20SH). Slip effect between the profile steel and the concrete flange was modelled by the interface elements (N6IF) at locations of the connectors. (Kulkarni and Li 2008) Detailed nonlinear shear force-slip relationship was adopted as the experimental reports for the modelled specimens (Amadio *et al*. 2004, Nie *et al*. 2008). Illustration of the meshing and reinforcing details of the FE models is given in Fig. 6.

A smeared crack approach is adopted for modelling the concrete. A crack is assumed to be initiated once the principal tensile stress in the concrete exceeds tensile strength of the concrete. After a crack is initiated, the fracture criterion is applied to determine whether the crack will propagate which is based on facture energy. Based on the model proposed by Hordijk which was implemented in the TNO Diana software (TNO Diana 2014), the fracture energy, G_f, is related to the zero-strength strain by (Fig. 7)

$$\varepsilon_{nn.ult}^{cr} = 5.136\frac{G_f}{h_c f_t} \tag{10}$$

in which h_c is the bandwidth of the cracks calculated as the cube root of the volume of an element.

After the crack opens, direction of the crack is assumed to be fixed and the constitutive relation of the cracked concrete is evaluated coaxial to direction of the crack. Concrete in compression was simulated with the parabolic compression model. (TNO Diana 2014) Diana software (TNO Diana 2014) considers effects of the lateral confinement or cracking by the model proposed by Vecchio (1983). The reinforcing steel and profile steel were modeled as idealized elastic until their characterized yield strain. After yield, behavior of the steel was modeled by their stress-strain curve reported. Amadio *et al*. (2004) and Nie *et al*. (2008) reported detailed shear force-slip relationship of the shear connectors in their specimens obtained from the pull-out test. These relationships were adopted for the interface elements for the corresponding models. Detailed

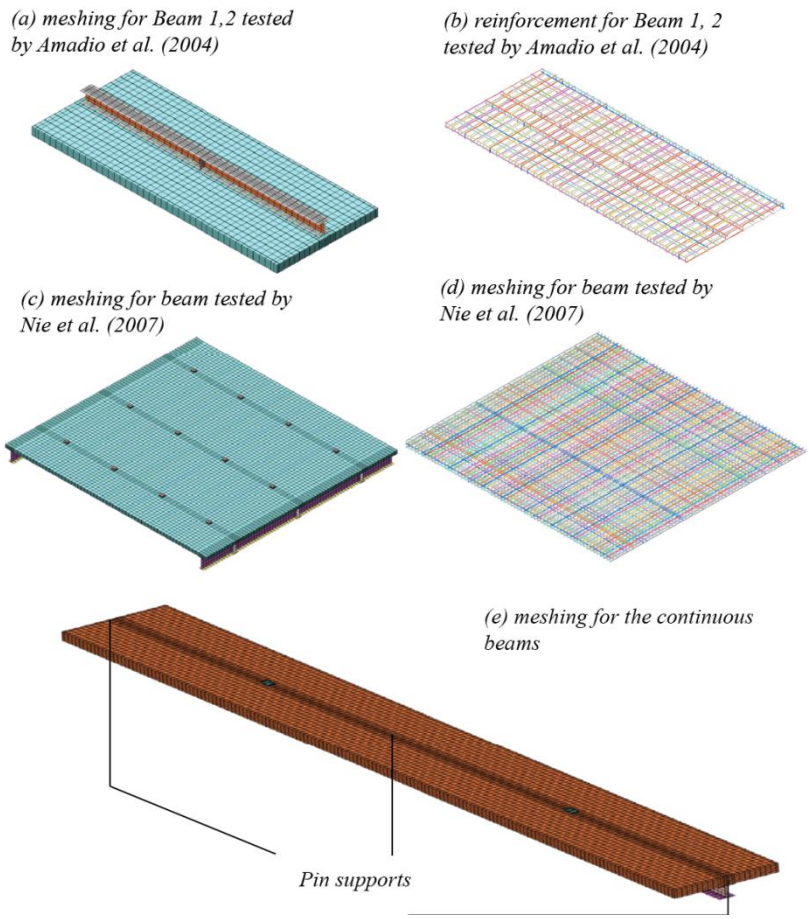

Fig. 6 Illustration of the meshing and reinforcing details of the FE models

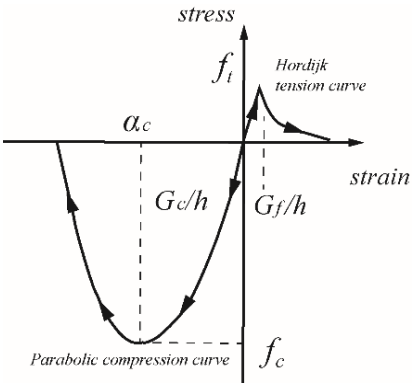

Fig. 7 Uniaxial stress-strain curve adopted for the concrete

parameters adopted for the FE models are reported in Table 2.

Fig. 8 shows comparisons of the experimental results with the FE results. The load-displacement curves of Beam 1 and Beam 2 tested by Amadio *et al*. (2004) are compared with the FE results in Figs. 8(a) and (b). The load-displacement curve of the beam tested by Nie *et al*. (2008) is given in Fig. 8(c) together with comparisons of the FE results in Fig. 8(d). Also compared are the FE and test derived sectional strain. For these specimens, the FE models predict their load-displacement curves accurately. The sectional strains of the FE models also approximate the experimental results at different load levels.

Table 2 Material parameters adopted for the FE models

	E_c (GPa)	f_c (MPa)	G_c (N/m)	f_t (MPa)	G_f (N/m)	f_y (MPa)
Beam 1 tested by Amadio *et al*. (2004)	34.3	36.1	51000	2.92	70	500 (Rebar) 253 (Profile steel)
Beam 2 tested by Amadio *et al*. (2004)	34.3	36.1	51000	2.92	70	500 (Rebar) 253 (Profile steel)
Beam tested by Nie *et al*. (2007)	27.5	30.3	43000	2.52	58	380 (Rebar) 295 (Profile steel)

*Note: E_c = Young's modulus for concrete, f_c = compressive strength for concrete,
G_c = fracture energy for concrete, f_t = tensile strength for concrete,
G_f = tensile fracture energy for concrete, f_y = yield strength for reinforcing and profile steel

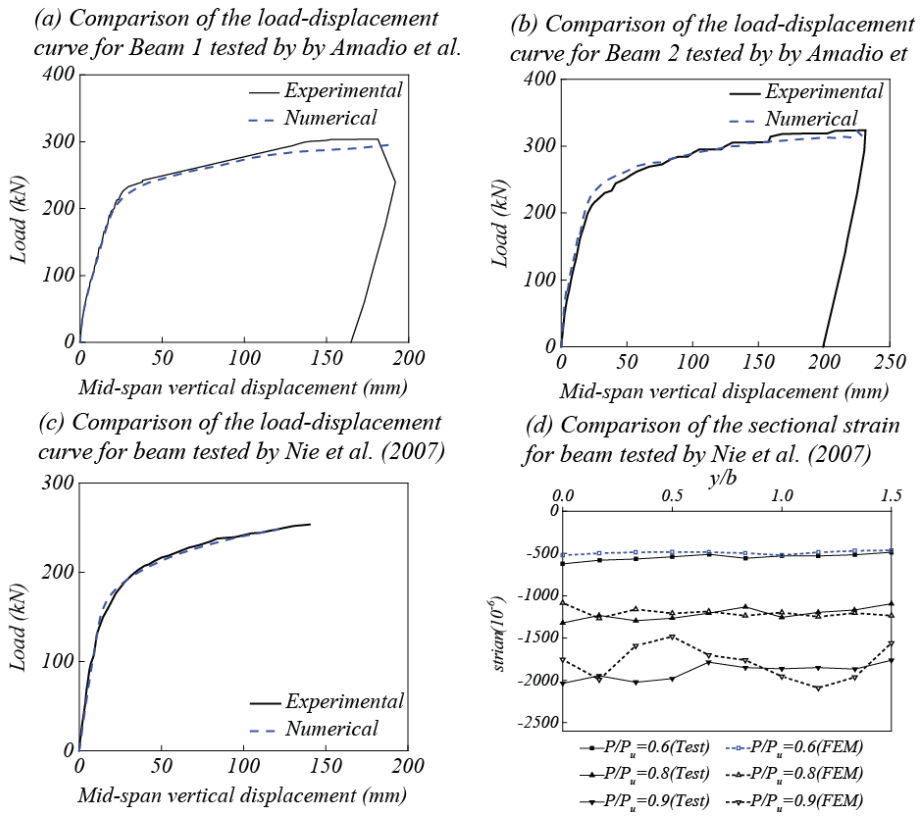

Fig. 8 Comparison of the predicted effective flange width with the reported width by Amadio *et al*. (2004)

3.2 Parametric study

Adopting the FE models, parametric studies were conducted regarding the parameters possibly related to the shear lag effect in steel-concrete composite beams. These models were modified from the model prototype (Beam 1 shown in Table 2 and Fig. 6) in different parameters. These parameters include the width of the flange, thickness of the flange, the transverse reinforcing ratio, the longitudinal reinforcing ratio and the grade of the concrete as summarized in Table 3. Specifically, the compressive strength, tensile strength and the Young's modulus of the concrete are all related to grade of the concrete. These parameters are modified simultaneously as shown in Table 3. Similar loading protocol was used for these models as the experimental test.

In addition to the one-span models geometrically similar with Beam 1, FE models are built for continuous steel-concrete composite beams with two spans as shown in Fig. 6. These models were built for investigating the shear lag effect in continuous beams with different loading conditions. They have similar reinforcing and material details with Beam 1, but span of these models were two times of the original beam span. They are supported with three pin supports with similar distance as shown in Fig. 6. Different load combinations were imposed to these models as summarized in Table 4.

4. Shear lag effect in steel-concrete composite beams with different configurations

4.1 Influences of the investigated design parameters

Results of the FE models are processed to calculate the R_{sle} ratio based on the longitudinal strains in the reinforcing bars from Eq. (9). The results of the FE models are given at different load levels corresponding to 60%, 80%, 100% and 105% of P_y, the minimal vertical force at yielding of the

Table 3 Parameters investigated by the FE models

Property name	Property value								
Width of the flange, B (mm)	640	960	1280	1600	1920	2240	2560	2880	3200
Longitudinal reinforcing ratio, ρ_l (%)	0.41	0.67	1	1.39	1.85	2.37			
Transverse reinforcing ratio, ρ_v (%)	0.236		0.652		1.31		2.62		
Thickness of the flange, t (mm)	80		100		120		160		
Grade of the concrete, f_c'(MPa)/f_t(MPa)/E_c(GPa)	20/2.2/27.1		30/2.9/30.6		40/3.5/33.3		50/4.1/35.6		

Table 4 Load combinations for the 2-span continuous beams

Model number	Description of the model	Illustration
B-2span-P1	Similar concentrated load P at x =-L/4 and x = L/2	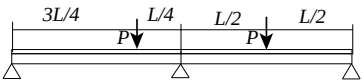
B-2span-P2	Concentrated load P at x = -L/2 and 2P at x = L/2	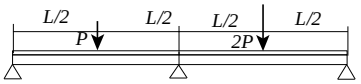
B-2span-P3	Evenly distributed load	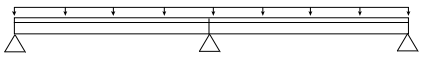

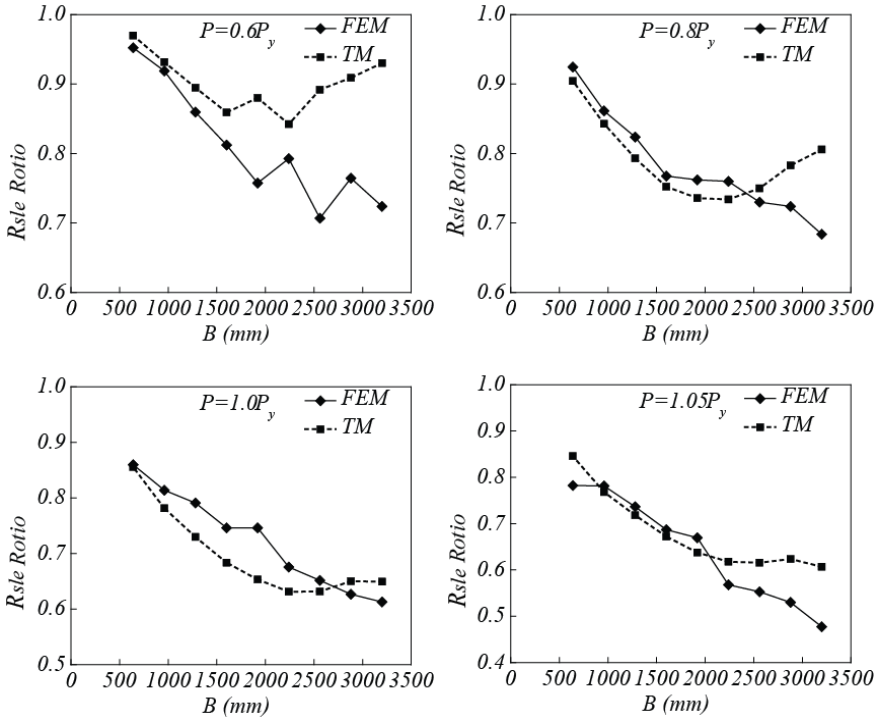

Fig. 9 Influences of the width of the concrete flange

longitudinal reinforcing bars. P_y was calculated based on the calculated strains in the reinforcing bars by the FE models. Compared with the FE model derived R_{sle} ratios and the calculated ratios by the proposed method based on the truss model (TM) in Figs. 9-13. In particular, H_{cr}, cracked span of the flange is related to vertical force applied to the beam. Therefore, the R_{sle} ratio calculated by TM is also related with the load level.

Expectedly, the width of the flange is found to be the most influential parameter to the shear lag effect. The R_{sle} ratio reduces with the increase of the width of the beam. When the width is 640 mm, the R_{sle} ratio is around 0.9. This is slightly less than the expected value based on the effective width specified by Eurocode 4 (ENV 1994-1-1 1994). Based on the design code, this flange width should be fully effective when span of the beam is 3800 mm. (ENV 1994-1-1 1994) When width of the flange is 3200 mm which approaches span of the beam, the R_{sle} ratio ranges from 0.4 to 0.7 depending on the load level. At yielding of the beam, the R_{sle} ratio is around 0.6 comparing with an effective width of 950 mm based on Eurocode 4. (ENV 1994-1-1 1994) It is clear that the current design code is quite conservative in considering the effect at yield load level.

The ratio of the longitudinal reinforcing bars, the ratio of horizontal reinforcing bars, thickness of the flange, and the grade of the concrete were also found to affect the shear lag effect. Among these ratios, increasing the longitudinal reinforcing ratio was found to increase the influences of the shear lag effect and reduce the R_{sle} ratio while increasing the horizontal reinforcing ratio, thickness of the flange and grade of the concrete were found to increase the R_{sle} ratio and reduce influences of the shear lag effect. those results are proved that the shear lag effect depends on the longitudinal and shear stiffness of the flange. Increasing the longitudinal reinforcing bars, decreasing the horizontal reinforcing bars and decreasing the grade of the concrete will lead to larger shear strains in the flange and correspondingly lower R_{sle} ratios. Apart from thickness of the flange, these ratios were not considered in the effective width definition of the current design codes. (ENV 1994-1-1 1994) However, they can be still influential. Increasing

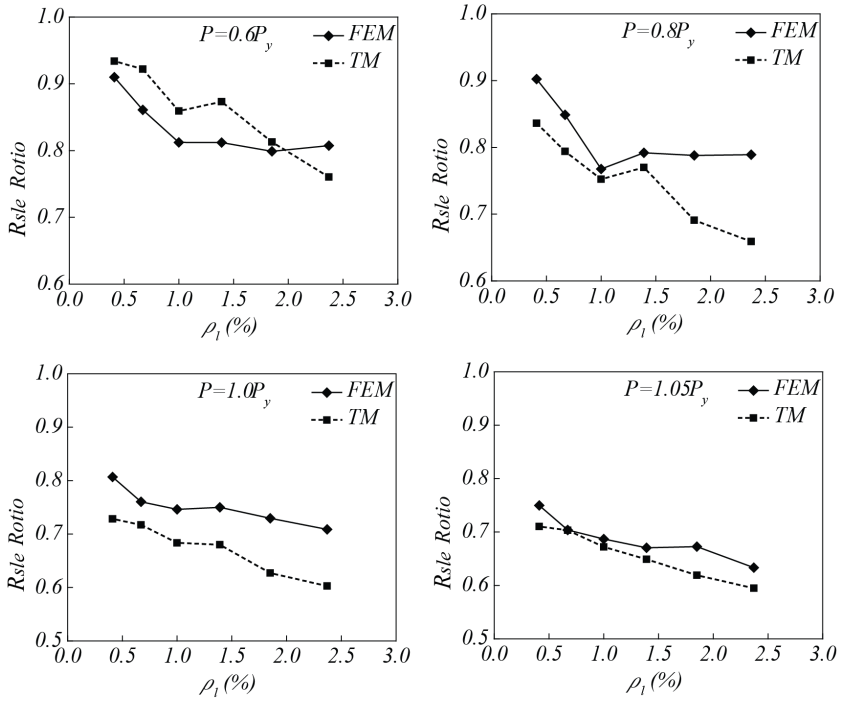

Fig. 10 Influences of the longitudinal reinforcing ratio

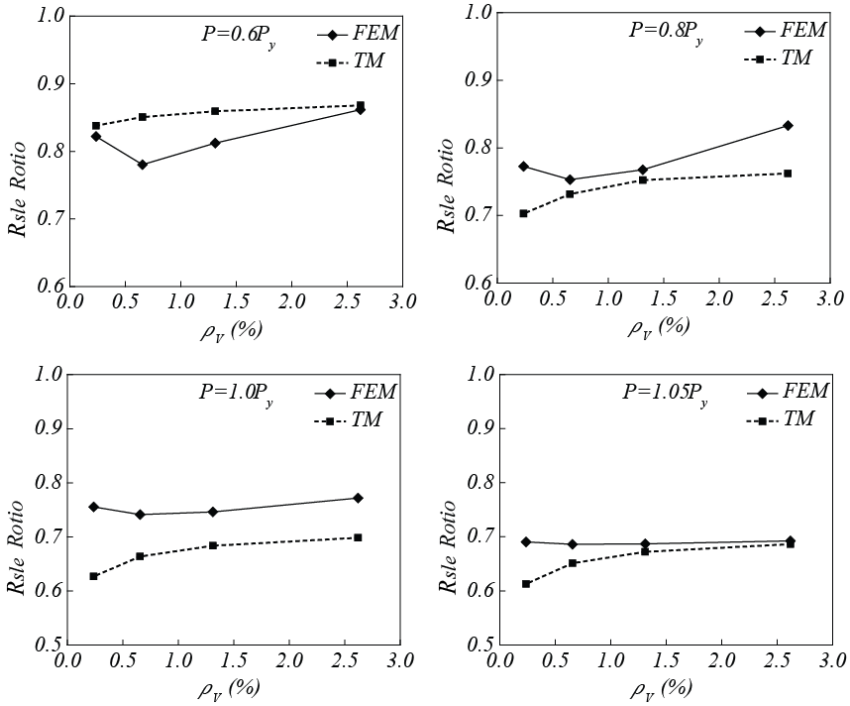

Fig. 11 Influences of the transverse reinforcing ratio

the longitudinal reinforcing ratio from 0.3% to 2.3% reduces the R_{sle} ratio at $1.05P_y$ from 0.83 to 0.71 while increasing thickness of the slab from 80 mm to 160 mm increases the R_{sle} ratio from 0.61 to 0.75.

In addition to the investigated design parameters, the load level of the beam affects the shear lag effect. As the vertical force increases from $0.6P_y$ to $1.05P_y$, the R_{sle} ratio generally reduces. This is in consisting with the experimental observations made by Amadio *et al*. (2004). As the width and scope of the cracks increases in the flange, shear stiffness of the flange decreases, and the shear lag effect becomes more distinct. In particular, the R_{sle} ratio was calculated based on strains of the longitudinal reinforcing bars instead of stress as shown in Eq. (9). After yielding of the reinforcing bars, it is expected that the tension force in the flange will be less sensitive to the strains and the flange

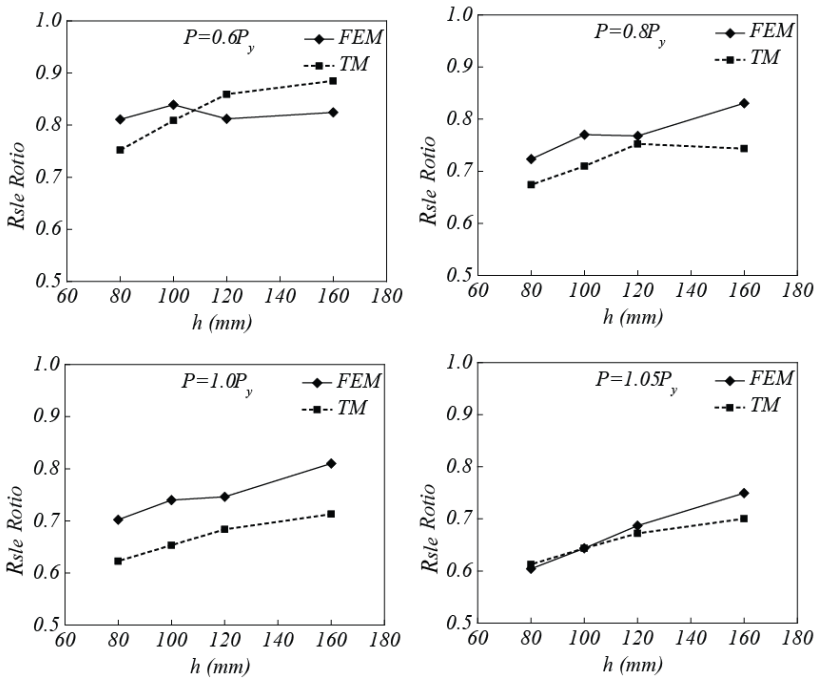

Fig. 12 Influences of the thickness of the flange

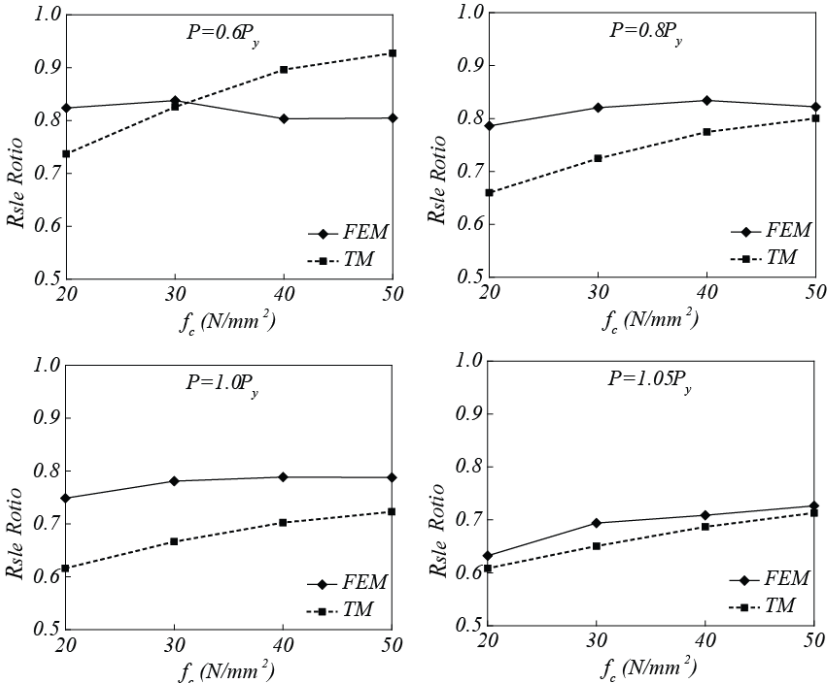

Fig. 13 Influences of the strength of the concrete

will become more effective. (Zhang and Li 2017, 2018)

Comparing the FE results with the ratios calculated by the proposed method, it can be seen that tendency of the R_{sle} affected by the investigated parameters can be predicted by the proposed method. Accuracy of the method depends on the load level. The proposed method was found to be most accurate corresponding to the load level of $1.05P_y$. This is probably related with the omission of the tension strengths of the concrete in deducing the method. This assumption is only true with well-developed cracks. At this load level, the maximum differences between the predicted and FE derived R_{sle} were within 30% of the FE calculated ratio. Relatively large error was found for the proposed method for models with width of the flange larger than 2500 mm. This is probably related to cracks in the flange. The FE and experimental results indicate that the flange may not be thoroughly cracked at first yield vertical force when the beam has a large flange width.

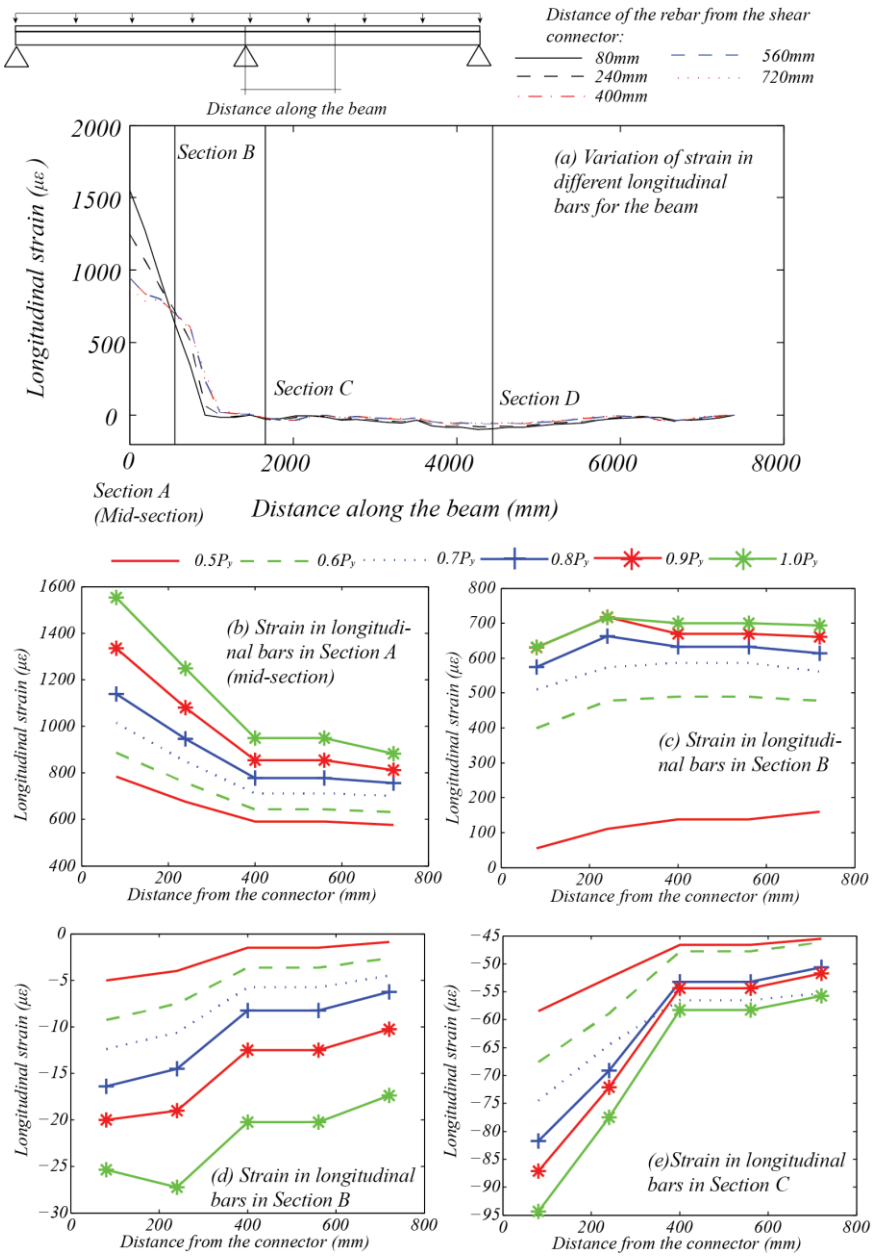

Fig. 14 Variation of the longitudinal strain along span of the beam and width of the flange

4.2 Shear lag effect in continuous beams

Hogging moments are mainly expected in continuous steel-concrete composite beams. In these beams, only the regions near the mid-span support are sustaining significant hogging moment while the other parts of the beam resist mainly sagging moment or very little hogging moment. Also, gravity load in different spans of the continuous beam may vary. Previous research investigations indicate that the shear lag effect may be very different along the span of the beam. (Chen *et al*. 2007) Additionally, the loading condition could influence the shear lag effect of the beam. (Zhang and Li 2018) Using the FE models, the shear lag effect in steel-concrete continuous beams with different loading conditions is investigated.

Fig. 14 summarizes the FE results of the longitudinal strain of the loaded 2-span model with evenly distributed load (B-2span-P3 shown in Table 4). Fig. 14(a) shows variation of the longitudinal strain along span of the beam. Due to symmetricity, results are given for only half of the beam span. Expectedly, large tension strains are observed at the middle support of the continuous beam. The longitudinal strain significantly reduces at locations away from the mid-section and compression strains are observed in most of the other parts of the beam. Figs. 14(b) to 14(e) shows variation of the longitudinal strain along width of the flange at different locations of the continuous beam. Comparing Figs. 14(b) and (c), it is clear that the shear lag effect in the hogging moment zone can be quite different. The mid-section is significantly affected by the shear lag effect, the longitudinal strain in the rebar furthest from the shear connector is 57% of that adjacent to the shear connector. For Section B with a 350 mm distance with the mid-section, on the other hand, the longitudinal strain in the

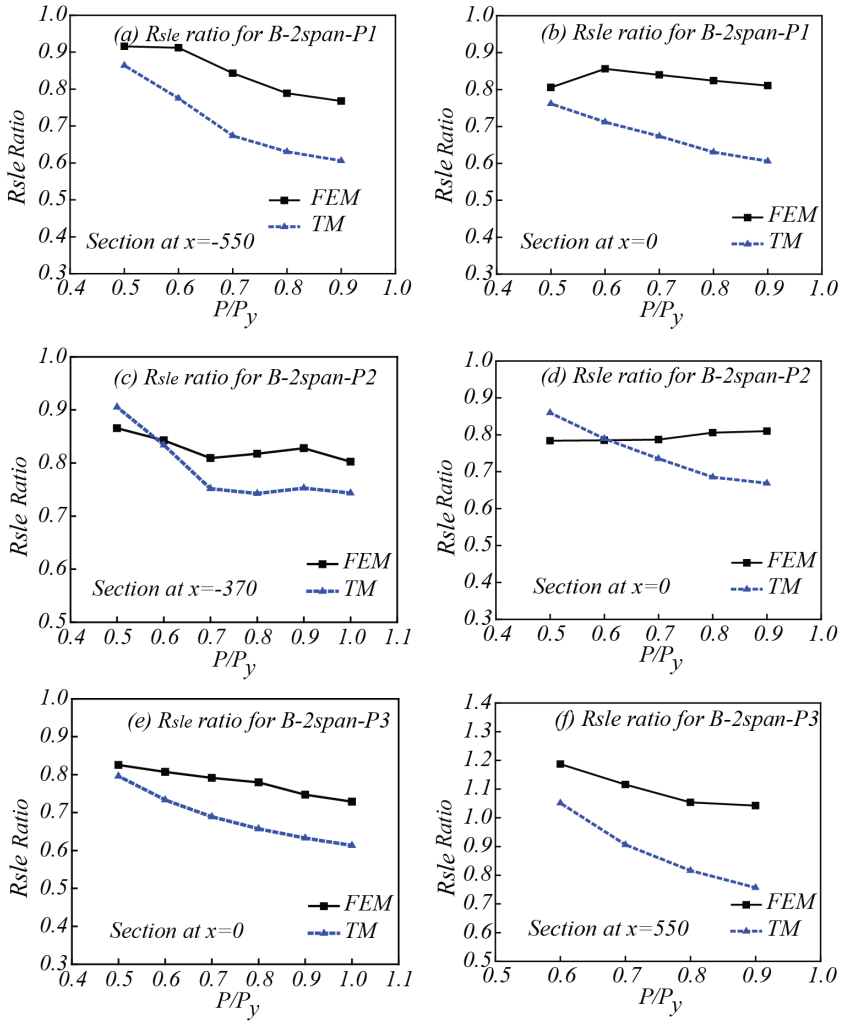

Fig. 15 Comparisons between the FE predicted and calculated R_{sle} ratio for continuous beams

rebars away from the shear connector is slightly larger than that adjacent to the connector which is similar with the negative shear lag effect observed in other concrete members. (Singh and Nagpal 1994, Zhang and Li 2018) Significant shear lag effect is also observed in the section sustaining sagging moment as shown in Figs. 14(d) and (e).

Fig. 15 compares the R_{sle} ratio predicted by the truss model with the FE results at different section, load levels and loading distributions. The proposed method was also used to calculate the R_{sle} ratio for these sections. Specifically, distribution of the shear force in the connectors is not symmetric around the midspan for the model B-2span-P2 which have unsymmetrical load. For this model, the shear force in the connector is approximately 0 at the section 370 mm left of the midspan based on the FE analysis. The proposed method was used and compared with the FE results at that section and the mid-span section respectively. The FE predicted R_{sle} ratios varies significantly at different sections and load levels. Generally, the FE predicted R_{sle} ratio reduces with increase of the load level. For different sections of the beam, variations of the R_{sle} ratio are very different for B-2Span-P3 with distributed loads compared with the two models with concentrated loads. For B-2Span-P1 and B-2Span-P2 with concentrated loads, variation of the R_{sle} ratio with span of the beam seems to be rather small. For B-2Span-P1, the R_{sle} ratio was around 0.8 for different sections. For B-2Span-P2, the R_{sle} ratio ranges from 0.9 to approximately 0.8 for the investigated sections. For the model with distributed load, on the other hand, the R_{sle} ratio increases significantly with span of the beam. At section with x = 550 mm, R_{sle} ratio larger than 1 was observed compared to the R_{sle} ratio of 0.75 to 0.8 at section with x = 0 mm. This tendency was predicted by the proposed method. Comparing the FE predicted ratio with the ratio predicted by the proposed truss model, slightly larger error can be found for the sections with a distance from the assumed bottom section. In these sections, the FE predicted R_{sle} ratio was underestimated. For the section with x = 550 mm for Model B-2span-P3, the proposed method predicts the R_{sle} ratio to range from 1.05 to 0.87 compared to the FE predicted ratio from 1.2 to 1.05. This is also probably related to the assumption of ignoring the tensile strength of the concrete in deducing the proposed method. For sections with a distance with the assumed bottom section, the cracks are not well developed and ignoring the tensile strength may underestimate shear stiffness of the concrete flange.

5. Conclusions

The shear lag effect in concrete flange of the steel-concrete composite beams sustaining hogging moment is investigated in this paper. A method for calculating the shear lag effect is proposed based on truss analogy. Results of the proposed method are compared with the experimental results and the FE results. Influences of the shear lag effect for steel-concrete composite beams are investigated with different design parameters, loading combinations and boundary conditions. Conclusions of the paper are summarized as following:

- The shear lag effect in steel-concrete composite beams sustaining hogging moment becomes severer with increase of the width of the flange, the longitudinal reinforcing ratio and become less significant with increase of the thickness of the flange, transverse reinforcing ratio and strength of the concrete. Additionally, the shear lag effect was found to be more severe with increase of the load until yielding of the beam.
- Based on the available experimental and FE results, the proposed method was found to predict the shear lag effect of composite beams affected by various parameters. The current data is limited to the composite beam slabs with common design configurations and a cubic concrete flange. Accuracy of the proposed method depends on load level of the beam and distribution of the shear connectors. The method was found to be most accurate around yielding of the beam.
- For continuous steel-concrete composite beams, influences of the shear lag effect significantly vary at different sections of the beam and negative shear lag effect can be observed. The tendencies of these variation were captured by the proposed method.

References

Amadio, C., Fedrigo, C., Fragiacomo, M. and Macorini, L. (2004), "Experimental evaluation of effective width in steel–concrete composite beams", *J. Constr. Steel Res.*, **60**(2), 199-220.

Aref, A.J., Chiewanichakorn, M., Chen, S.S. and Ahn, I.S. (2007), "Effective slab width definition for negative moment regions of composite bridges", *J. Bridge Eng.*, **12**(3), 339-349.

Beyer, K., Dazio, A. and Priestley, N. (2011), "Shear deformations of slender reinforced concrete walls under seismic loading", *ACI Struct. J.*, **108**(EPFL-ARTICLE-162084), 167-177.

Bezerra, L.M., Bonilla Rocha, J.D., Mirambell Arrizabalaga, E. and Massicotte, B. (2018), "Review of stud shear resistance prediction in steel-concrete composite beams", *Steel Compos. Struct., Int. J.*, **27**(3), 355-370.

Boules, P.F., Mehanny, S.S. and Bakhoum, M.M. (2018), "Shear lag effects on wide U-section pre-stressed concrete light rail bridges", *Struct. Eng. Mech., Int. J.*, **68**(1), 67-80.

Carpenter, J.A., Chen, S.S., Aref, A.J., Chiewanichakorn, M., Ahn, I-S., Nottis, A. and Kalpakidis, I. (2005), "Effective slab width for composite steel bridge members", Report No. 543; Department of Civil, Structural and Environmental Engineering, State University of New York at Buffalo, NY, USA.

Castro, J.M., Elghazouli, A.Y. and Izzuddin, B.A. (2007), "Assessment of effective slab widths in composite beams", *J. Constr. Steel Res.*, **63**(10), 1317-1327.

Chen, S.S., Aref, A.J., Chiewanichakorn, M. and Ahn, I.S. (2007), "Proposed effective width criteria for composite bridge girders", *J. Bridge Eng.*, **12**(3), 325-338.

Chiewanichakorn, M., Aref, A.J., Chen, S.S. and Ahn, I.S. (2004), "Effective flange width definition for steel–concrete composite bridge girder", *J. Struct. Eng.*, **130**(12), 2016-2031.

Chiorean, C.G. and Buru, S.M. (2017), "Practical nonlinear inelastic analysis method of composite steel-concrete beams with partial composite action", *Eng. Struct.*, **134**, 74-106.

Dezi, L., Gara, F. and Leoni, G. (2003), "Shear-lag effect in twin-girder composite decks", *Steel Compos. Struct., Int. J.*, **3**(2), 111-122.

Ding, F.X., Liu, J., Liu, X.M., Guo, F.Q. and Jiang, L.Z. (2016), "Flexural stiffness of steel-concrete composite beam under positive moment", *Steel Compos. Struct., Int. J.*, **20**(6), 1369-1389.

El-Shihy, A.M., Fawzy, H.M., Mustafa, S.A. and El-Zohairy, A.A. (2010), "Experimental and numerical analysis of composite beams strengthened by CFRP laminates in hogging moment region", *Steel Compos. Struct., Int. J.*, **10**(3), 439-453.

ENV 1994-1-1 (1994), Eurocode 4, Design of composite steel and concrete structures, BSI; UK.

Fang, G., Wang, J., Li, S. and Zhang S. (2016), "Dynamic characteristics analysis of partial-interaction composite continuous beams", *Steel Compos. Struct., Int. J.*, **21**(1), 195-216.

Gao, Y., Zhou, Z., Liu, D. and Wang, Y. (2016), "Cracking of a prefabricated steel truss-concrete composite beam with pre-embedded shear studs under hogging moment", *Steel Compos. Struct., Int. J.*, **21**(5), 981-997.

Gara, F., Carbonari, S., Leoni, G. and Dezi, L. (2014), "A higher order steel–concrete composite beam model", *Eng. Struct.*, **80**, 260-273.

Goncalves, R. and Camotim, D. (2010), "Steel-concrete composite bridge analysis using generalised beam theory", *Steel Compos. Struct., Int. J.*, **10**(3), 223-243.

Henriques, D., Gonçalves, R. and Camotim, D. (2015), "A physically non-linear GBT-based finite element for steel and steel-concrete beams including shear lag effects", *Thin-Wall. Struct.*, **90**, 202-215.

Hines, E.M. and Seible, F. (2004), "Web crushing capacity of hollow rectangular bridge piers", *ACI Struct. J.*, **101**(4), 569-579.

Ju, H., Lee, D.H., Hwang, J.H., Kang, J.W., Kim, K.S. and Oh, Y.H. (2013), "Torsional behavior model of steel-fiber-reinforced concrete members modifying fixed-angle softened-truss model", *Compos. Part B: Eng.*, **45**(1), 215-231.

Kim, J.H. and Mander, J.B. (1999), "Truss modeling of reinforced concrete shear-flexure behavior", Technical Report No. Mceer-99-0005; Multidisciplinary Center for Earthquake Engineering Research, Buffalo, NY, USA.

Kim, J.H. and Mander, J.B. (2007), "Influence of transverse reinforcement on elastic shear stiffness of cracked concrete elements", *Eng. Struct.*, **29**(8), 1798-1807.

Kulkarni, S.A. and Li, B. (2008) "Finite Element Analysis of Precast Hybrid-Steel Concrete Connections under Cyclic Loading", *J. Constr. Steel Res.*, **64**, 190-201.

Kwan, A.K.H. (1996), "Shear lag in shear/core walls", *J. Struct. Eng.*, **122**(9), 1097-1104.

Lasheen, M., Shaat, A. and Khalil, A. (2018), "Numerical evaluation for the effective slab width of steel-concrete composite beams", *J. Constr. Steel Res.*, **148**, 124-137.

Lee, C.K. and Chiew, S.P. (2013), "An efficient modified flanges only method for plate girder bending resistance calculation", *J. Constr. Steel Res.*, **89**, 98-106.

MacGregor, J.G., Wight, J.K., Teng, S. and Irawan, P. (1997), *Reinforced Concrete*: *Mechanics and Design* (*Vol*. *3*), Prentice Hall, Upper Saddle River, NJ, USA.

Moffatt, K.R. and Dowling, P.J. (1978), "British shear lag rules for composite girders", *J*. *Struct*. *Div*.*-ASCE*, **104**(7), 1123-1130.

Moharrami, M., Koutromanos, I., Panagiotou, M. and Girgin, S. (2015), "Analysis of shear-dominated RC columns using the nonlinear truss analogy", *Earthq*. *Eng*. *Struct*. *D*., **44**(5), 677-694.

Nie, J.G., Cai, C.S., Zhou, T.R. and Li, Y. (2007), "Experimental and analytical study of prestressed steel–concrete composite beams considering slip effect", *J*. *Struct*. *Eng*., **133**(4), 530-540.

Nie, J.G., Tian, C.Y. and Cai, C.S. (2008), "Effective width of steel–concrete composite beam at ultimate strength state", *Eng*. *Struct*., **30**(5), 1396-1407.

Pan, Z. and Li, B. (2013), "Truss-Arch Model for Shear Strength of Shear-Critical Reinforced Concrete Columns" *ASCE J*. *Struct*. *Eng*., **139**(4): 548-560.

Pan, Z., Li, B. and Lu, Z. (2014), "Effective shear stiffness of diagonally cracked reinforced concrete beams", *Eng*. *Struct*., **59**(2), 95-103.

Paulay, T. (1971), "Coupling beams of reinforced concrete shear walls", *J*. *Struct Div*.*-ASCE*, **97**(3), 843-862.

Pecce, M., Rossi, F., Bibbo, F.A. and Ceroni, F. (2012), "Experimental behaviour of composite beams subjected to a hogging moment", *Steel Compos*. *Struct*., *Int*. *J*., **12**(5), 395-412.

Qi, J., Wang, J., Li, M. and Chen, L. (2017), "Shear capacity of stud shear connectors with initial damage: Experiment, FEM model and theoretical formulation", *Steel Compos*. *Struct*., *Int*. *J*., **25**(1), 79-92.

Siekierski, W. (2015), "Equivalent moment of inertia of a truss bridge with steel-concrete composite deck", *Struct*. *Eng*. *Mech*., **55**(4), 801-813.

Singh, Y. and Nagpal, A.K. (1994), "Negative shear lag in framed-tube buildings", *J*. *Struct*. *Eng*., **120**(11), 3105-3121.

Sun, Q., Yang, Y., Fan, J., Zhang, Y. and Bai, Y. (2014), "Effect of longitudinal reinforcement and prestressing on stiffness of composite beams under hogging moments", *J*. *Constr*. *Steel Res*., **100**, 1-11.

TNO Diana (2014), *Finite Element Analysis User's Manual-Release 9.6 TNO DIANA*, Delft, The Netherlands.

Vecchio, F.J. (1983), *The Response of Reinforced Concrete to In-Plane Shear and Normal Stresses*, University of Toronto, Ontario, Canada.

Vecchio, F.J. and Collins, M.P. (1986), "The modified compression-field theory for reinforced concrete elements subjected to shear", *ACI J*., **83**(2), 219-231.

Xiang, Y. and He, X. (2017), "Short-and long-term analyses of shear lag in RC box girders considering axial equilibrium", *Struct*. *Eng*. *Mech*., *Int*. *J*., **62**(6), 725-737.

Yang, Y., Yu, Y., Zhou, X., Roeder, C.W. and Huo, X. (2016), "Study on mechanical performance of composite beam with innovative composite slabs", *Steel Compos*. *Struct*., *Int*. *J*., **21**(3), 537-551.

Zhang, Z. and Li, B. (2017), "Shear lag effect in tension flange of RC walls with flanged sections", *Eng*. *Struct*., **143**, 64-76.

Zhang, Z. and Li, B. (2018), "Effects of the shear lag on longitudinal strain and flexural stiffness of flanged RC structural walls", *Eng*. *Struct*., **156**, 130-144.

Zhong, X., Zhang, T., Shu, X. and Xu, H. (2017), "Shear-lag behavior of prestressed concrete box-girder bridges during balanced cantilever construction", *Adv*. *Concr*. *Constr*., **5**(5), 469-479.